CHAPTER 1

Introduction

1.1 Catalyst [1]

Catalyst is known as a substance helping to reduce the potential energy barrier in the reaction pathway while catalysis is defined as its corresponding kinetic phenomenon. The performance of catalyst is usually determined by a turn-over rate. A turn-over rate is measured by detecting an amount of reactant molecules which are converted on the active site per a unit of catalytic surface area per second at specific conditions (temperature, pressure and concentrations of reactant and product). By multiplying the specific rate with the reaction time used in the study, the turn-over number can be obtained. Since the catalytic action occurs at specific sites on solid surface which often called 'active sites', it can be implied that the high catalytic efficiency depends on the specific surface area. It is generally believed that high surface area of catalyst can increase the rate of reaction. The turn-over number must be greater than unity to assure that the reaction is catalytic (i.e., that there is more than one 'turnover'). If the turn-over number is less than unity, we may be dealing with a stoichiometric reaction where the solid surface may be acting as a reactant rather than a catalyst.

1.2 Catalysis on semiconductor

1.2.1 Semiconductors [1]

The intrinsic semiconductor is typically composed of completely filled electrons in the valence band and there is a band gap which is in the range between 1–3 eV. The electrons might be excited to the conduction band leaving an empty orbital in valence band. In the semiconductor, the electrical conductivity exponentially increases with

increasing temperature, while in the metal the conductivity drops slowly due to random thermal motion.

Doping or adding impurities can also increase the electrical conductivity of the semiconductor. The electron on the donor level (n-type semiconductor) can be excited into the conduction band. The hole appears at the valence band by transferring of electron to the acceptor level (p-type semiconductor). The free electron and hole are generated in the doped semiconductor, so more conductivity was detected. Moreover, the coupling system between two semiconductors can also enhance the conductivity of the semiconductors. An improved electron-hole transfer or photogenerated charge transfer could enhance the chemisorption between the adsorbate and surface, which is beneficial to an increased photocatalytic performance.

1.2.2 Direct and indirect bandgap [2]

The photon absorption rate depends on the band structure of solid. The energy-electron wave vector (E-k) diagrams of the direct and indirect band gaps of solid are illustrated in Fig 1.1(a) and 1.1(b) respectively. The nature of band gap can be classified according to the conservation of momentum. From Fig 1.1(a), it can be implied that the electron wave vector with no change in electron momentum during a photon absorption process is considered to be the direct band gap which represents photon absorption by vertical line on E-k diagrams. It is immediately apparent from the indirect band gap in Fig 1.1b that the electron wave vector significantly changes its momentum in the absorption process. It is not possible to make this jump by absorption of a photon alone because the transition must involve with phonon to conserve momentum, while the direct band gap absorption can occur without phonon being involved.

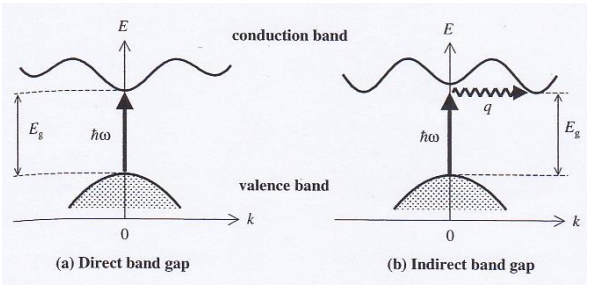

Fig. 1.1 E-k diagram of direct (a) and indirect (b) band gap semiconductors [2].

1.2.3 Band theory: metals, semiconductors and insulators [2]

The atom in a solid (metals, semiconductors or insulators) are packed very close to each other with the interatomic separation approximately equal to the size of the atoms. The outer orbitals of the atoms overlap and strongly interact with each other. However, since the inner core orbitals do not overlap, they remain discrete even in the solid state. This causes the discrete energy levels of the free atoms to be broadened into band, as shown schematically in Fig 1.2. Optical transition can occur between these electronic bands. This process is called interband absorption. By absorbing a photon, the electron can jump from the lower level band to the one above it or from valence band to conduction band. The excitation of the electron leaves unoccupied valence band and electron in the final state which is equivalent to the creation of a hole and an electron respectively. Therefore, the electron-hole pair is formed in the process.

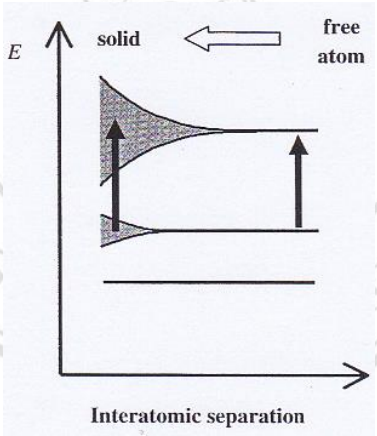

Fig. 1.2 Broaden band energy level of overlapped outer atoms of solid [2].

Electrons are generally filled in the energy bands up to the Femi energy (E_F), which is determined by the total electron density. Fig. 1.3(a) shows a schematic energy diagram for a monovalent metal such as sodium, or a trivalent metal such as aluminium. These materials have an odd number of electrons per atom, which means that the highest occupied band will only be half full. The Femi energy will lie in the middle of the highest occupied band. Electrons with energy just below the Femi level can easily be excited to the empty state just above E_F. This makes it easy to accelerate the electrons with an electric field and explains why metals are good electrical conductors.

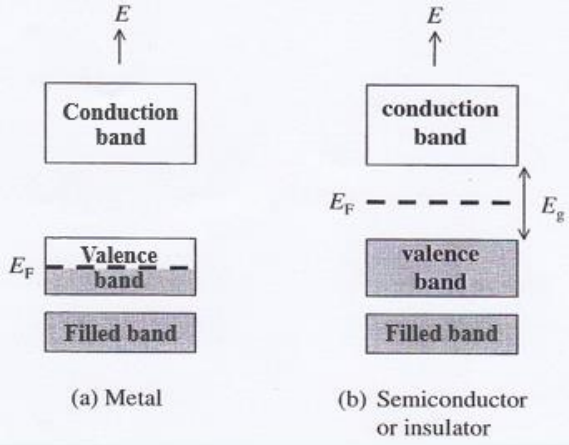

Fig. 1.3 Continuous band energy of metal (a) and discrete band energy level of semiconductors or insulators (b) [2].

Fig 1.3(b) shows the equivalent energy level diagram for a semiconductor such as silicon or an insulator such as diamond. These elements have an even number of electrons per atom, and the highest occupied band is full of electrons. This highest occupied band is called the valence band, while the lowest unoccupied band is called the conduction band. The Femi level lies somewhere within the energy gap between the valence band and conduction band. The first empty state for the electrons are in the conduction band, and it requires a minimum amount of energy equal to the band gap energy (E_g) to excite the electrons to the available state. This makes it very difficult to accelerate electrons when an external electric field is applied and inhibits the flow of electric current through the sample. Therefore, semiconductors and insulators have much lower electrical conductivity than metals. The distinction between an insulator and a semiconductor is related to the size of band gap. Semiconductors have smaller band gaps than insulators which are in the range between 1-3 eV, while the insulators has band gap energy about 4-12 eV at 0 K [3].

As a result of the small E_g of semiconductor, a significant number of electrons can be excited from the valence band to the conduction band at room temperature in the semiconductor material.

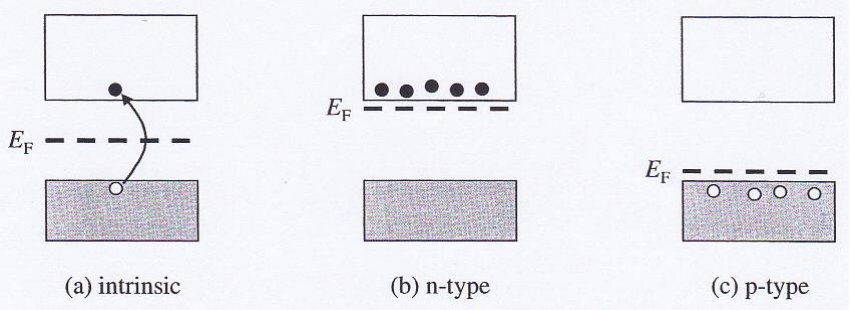

Fig. 1.4 Band energy diagram of intrinsic semiconductors (a) and extrinsic semiconductors of n-type (b) and p-type (c) doping [2].

Fig 1.4(a) shows the intrinsic semiconductors with no doping thus the Femi level located in the middle between conduction band and valence band, while Fig. 1.4(b) applies to a crystal with n-type doping. In this case, impurities with extra electrons are deliberately introduced into the crystal. For example, the n-type semiconductor can be obtained by adding atoms from group V of the periodic table into the crystal structure of group IV. Semiconductors such as silicon and germanium which come from group IV, have four valence electrons per atom. The impurities donate one extra electron for each dopant atom. These extra electrons lie in donor levels just below the conduction band. The electron state are filled up to the donor levels, so the Femi level energy must lie very close to the donor level energies as shown in Fig 1.4(b). The electrons in the donor level can be easily excited into the conduction band at room temperature and the electrical properties of the n-type materials are determined by these extrinsic electrons arising from the impurity atoms.

For the p-type doping as shown in Fig 1.4(c), group III atoms are doped into the crystal structure of group IV during its growth. These atoms have a deficit of one electron per atom compared to four-valent atoms that make up the bulk of the crystal. Each impurity atom can accept one electron from the valence band. The acceptor levels are just above the top of the valence band that electrons can easily be excited to these empty states at room temperature. This creates a population of free holes in the valence band which determines the extrinsic electrical conductivity of the sample. The Femi level approximately coincides with the acceptor energy because the states up to the acceptor levels are filled with electrons.

1.3 Photocatalysis [1,4]

1.3.1 Classification of photocatalysis

The catalytic reaction can be generally classified as homogeneous and heterogeneous processes depending on the physical form of reactant and catalyst. There are both advantages and disadvantages for the two processes. However, the heterogeneous catalysis is favorably employed. A comparison between two catalytic processes is shown in Table. 1.1.

Table 1.1 Comparison between homogeneous ad heterogeneous catalysis [modified from 1].

Contents	Homogeneous catalysis	Heterogeneous catalysis
Activity	high	variable
Selectivity	high	variable
Reaction conditions	mild	harsh
Life of catalyst	variable	long
Catalyst recycling	expensive	not necessary

From the comparison above, it was found that a heterogeneous catalytic system is chemically robust and easier to collect after use by centrifugation which is less expensive, thus making it possible to recycle. Therefore, the heterogeneous catalysis has been used in this research.

1.4 Redox reaction in photocatalysis [1]

In the heterogeneous system, the band theory and electronic theory of catalysis have intensively been studied in order to understand the photo-processes in semiconductor systems. The occurrence and the efficiency of various photo-redox processes are intimately related to the position of valence and conduction band edges. From the nature of semiconductor, the energy level of the lower edge of conduction band is indicative of a reductive strength of the photoexcited electrons; whereas the upper edge of valence band is indicative of an oxidative strength of photogenerated holes. Based on the reduction potential of these valence and conduction band edges, the system can be

classified into 4 groups from the view point of water splitting reaction as shown in Fig. 1.5.

1.4.1 Oxidation-Reduction type: the oxidation power of holes in the valence band is strong enough to oxidize water to produce O_2 since the valence band located at a more positive potential energy than the O_2/H_2O level. The reduction power of electrons in the conduction band are also strong enough to reduce H^+ to produce H_2 since the conduction band locates at more negative potential energy than H^+/H_2 level. Therefore, this type can produce both O_2 and H_2 such as in the case of TiO_2, $SrTiO_3$ and CdS photocatalysts.

1.4.2 Reduction type: only reduction is strong enough to reduce water and form H_2; while the oxidation power is too weak such as CdTe, CdSe and Si.

1.4.3 Oxidation type: only the oxidation power is strong enough to oxidize water such as WO_3, Fe_2O_3 and Bi_2O_3.

1.4.4 X-type: the conduction band and the valence band locate between the H^+/H_2 and O_2/H_2O levels, so oxidation and reduction is not occurred and neither O_2 nor H_2 can be produced.

In the photocatalysis, the photon with energy higher than the band gap energy ($E>E_g$) can generate electron-hole pairs at conduction band and valence band respectively. The generated charge carriers will move under the influence of electric field into the bulk or the surface of semiconductor, leading to a separation of charge carriers. This resulting non-equilibrium distribution of electrons and holes then leads to occurring reduction and oxidation processes.

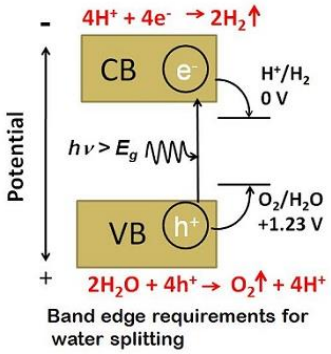

Fig. 1.5 Redox reaction in photocatalysis from the view point of water splitting reaction for the evolution of H_2 and O_2 molecules [5].

1.5 Enhancement of photocatalysis [1]

For an enhancement of charge separation, metallization or coupling between two semiconductors are generally performed.

1.5.1 Metallization

The presence of metal in semiconductor used as photocatalyst usually increases the efficiency of semiconductor. The enhanced activity can be ascribed to high electron affinity of metal for trapping the photoexcited electrons to perform subsequent reduction reaction and trapping holes in oxidation reaction; thereby increasing overall efficiency of the process. The metallization is usually carried out by impregnation method using an aqueous solution containing the corresponding metallic salt. Generally, the extent of metal loaded is in the range of 0.1-1.0 wt%. An excessive loading can lead to a formation of electron-hole recombination center, hence a fast recombination rate as a consequence.

1.5.2 Coupling of semiconductors

Another interesting approach is to combine two semiconductors together, this method can improve charge separation by inter-particles electron-hole transferring mechanism.

1.6 Model of heterogeneous catalysis [1,6]

Many kinetic studies on the heterogeneous catalysis reveal that the heterogeneous catalysis is usually related to the Langmuir-Hinshelwood model which is illustrated by the following simplified fictitious case of a bimolecular reaction based on competitive monolayer occupation of surface sites by two adsorbed reactants. Adsorption and desorption steps are usually assumed to be in equilibrium and the reaction is considered as one surface reaction step which is very low (hence irreversible) and can be used to determine the reaction rate.

Langmuir-Hinshelwood mechanism assumes that the rate of heterogeneous reaction is controlled by the reaction of the adsorbed molecules, while all of adsorption and

desorption processes are in equilibrium. The Langmuir model is based on the following assumptions [7]:

1. Adsorption proceeds only until a single adsorption layer is formed (monolayer)
2. All sites are equivalent, i.e. the surface is homogeneous; and the adsorbed molecules do not influence one another.

Let A(g) and B(g) be reactant gas molecules that adsorb (and desorb) rapidly on the surface (surface species are labeled *A and *B). They react with free surface sites (*) as shown in Eq. 1.1.

$$A_{(g)} + * \underset{k_d}{\overset{k_a}{\Leftrightarrow}} * A \qquad (1.1)$$

where k_a and k_d are rate constants for adsorption and desorption and $K_A = k_a/k_d$ is the adsorption equilibrium constant for A(g). On the surface, these adsorbed species diffuse freely and on meeting each other react slowly (*A + *B → X) to form the substrate material, X.

1.7 Steps in heterogeneous reactions [1]

To understand the mechanism of catalytic reaction, there are several consecutive reaction steps in which the slowest one could be the rate determining step in overall catalytic reaction.

[a] Diffusion of reactants to the surface
[b] Adsorption of reactant at the surface
[c] Chemical reaction on the surface; molecular rearrangements at active surface sites
[d] Desorption of products from the surface
[e] Diffusion of products away from the surface.

Normally the reaction step [c] is considered to be the rate limiting, whereas in some cases, step [b] and [d] are found to be the rate determination step according to this following correlations.

Rate of diffusion $\alpha\ T^{1/2}$

Rate of reaction $\alpha\ e^{T}$ from Arrhenius equation ($k = Ae^{-Ea/RT}$)

While

T	=	temperature (K)
k	=	specific rate constant
A	=	frequency factor
E_a	=	energy of activation
R	=	gas constant (8.314 J $mol^{-1}K^{-1}$ or 0.0821 L atm $mol^{-1}K^{-1}$)

1.8 Physical adsorption and chemisorption [1]

Owing to unsaturated coordination sphere of the atoms at surface, the incoming gas molecules can form bonding interaction. It was found that an increased concentration of gas molecules in the immediate vicinity of the surface appeared. This preferential accumulation of gas molecules at the surface is called adsorption. In a heterogeneous reactions catalyzed by solid, at least one of the reactants must be attached for a significant period of time to the surface of the solid catalyst. This can be achieved through the phenomenon of adsorption.

Since the adsorption is thermodynamically a spontaneous process, it should be accompanied by a decrease in the free energy of the system. When the gas molecules are adsorbed from the gas phase, it loses certain degree of freedom (one or more degrees of translational and rotational motion) and hence, the process is attended with a decrease in entropy, or ΔS is negative. Therefore, it is clear from thermodynamic relation in Eq. 1.2 that the adsorption is exothermic reaction.

$$\Delta G = \Delta H - T\Delta S \qquad (1.2)$$

The adsorption process can be divided into two types, physical adsorption and chemisorption according to the forces involved in the binding at the surface. Physical adsorption results from intermolecular forces which normally arise from the interaction of permanent dipoles. For this reason, physical adsorption is also known as Van Der Walls adsorption which can occur with any system of gas and solid under the suitable conditions of temperature and pressure. On the other hand, chemisorption involves rearrangement of the electron of interacting gas (adsorbate) and the solid (adsorbent)

resulting in the formation of chemical bonds. Therefore, chemisorption will take place only when the gas is capable to form chemical bonding. To distinguish between two types of interaction, several criteria are summarized in Table 1.2**.**

Table 1.2 Differences between physisorption and chemisorption [1].

Criteria	**Physical adsorption**	**Chemisorption**
Heat of gas adsorption	Low	High
Specificity	Low	High
Reversibility	Removed at the same temperature at adsorption by decreasing pressure	Severe conditions with high temperature
Extent of adsorption	Multilayers	Mono-molecular layer
Pressure dependence of adsorption	Pressure and temperature close to the liquefaction	Much lower pressure and much higher temperature
Rate of adsorption	Rapidly (no activation required)	Slowly (required activation)

1.9 Kinetics of heterogeneous catalytic reactions [8]

1.9.1 The pseudo-first order reactions

In general the reaction A + B → products has rate equation in this following form (Eq. 1.3).

$$\text{Rate} = k\,[\text{A}]^{\alpha}\,[\text{B}]^{\beta} \qquad (1.3)$$

where α is the reaction order with respect to A and β is the reaction order with respect to B, while the total order is $n = \alpha + \beta$.

If the effect of [B] on the rate is kept constant or keeping its concentrations in large excess over another reactant throughout the reaction, then the effect of [A] on the rate could be studied independently of [B]. Therefore, $[B]^{\beta}$ term is also effectively constant throughout the reaction which can be taken with k to give this following rate equation where k' is called the pseudo-first order rate constant (Eq. 1.4-1.6).

$$\text{Rate} = k'\,[A]\,\alpha \qquad (1.4)$$

While $k' = k\,[B]^{\beta}$ (1.5)

Therefore $\log k' = \log k + \beta \log [B]$ (1.6)

A plot of log k' versus log [B] should be linear with the slope of β and the intercept on y-axis is log k.

Since the kinetics of heterogeneous catalysts adsorption follows a Langmuir-Hinshelwood mechanism, the reaction rate varies proportionally with the coverage. The Langmuir-Hinshelwood kinetics equation can be expressed as in Eq. 1.7 [9-10]:

$$\ln \frac{C_0}{C} + K(C_0 - C) = k_r K t \tag{1.7}$$

where C_0 is the initial concentration of the reactant, K is the adsorption equilibrium constant, C is the concentration of the adsorbate, and k_r is the reaction rate constant. For dilute solutions, KC becomes less than 1 and the reaction is of the apparent first order as shown in Eq. 1.8 [9-10].

$$\ln \frac{C_0}{C} = kt \tag{1.8}$$

where k is the rate constant of first order reaction.

1.10 Catalyst deactivation [1]

Catalyst is usually defined as an accelerated substance of the chemical reaction without getting affected or changed after reactions, so the catalyst can be considered ideally as an infinite life time material. However, in practice all catalysts deactivate at different rate and have finite lives. These deactivations are often a result of side reaction which can occur parallel to the desired reaction or poisoning. The two main processes leading to catalyst deactivation are as follows.

1.10.1 Poisoning (chemical effect): poisoning can occur from strong chemisorption of impurities, reactants, products or by-products. This deactivation will block the active site of catalyst, therefore the interaction between adsorbed species and catalyst surface is not possible.

1.10.2 Thermal degradation: catalytic activity is lost due to heating process which is a serious problem for metal oxide catalysts. During the thermal

treatment, the catalyst will lose some surface area owing to crystallite growth and collapsed pores, so the catalytic phase was transformed into a non-catalytic phase.

1.11 Heterojunction [11]

Many interesting researches on heterojunction have focused on the electrical and optical properties of the heterostructure system. The two coupled materials can either be metal-semiconductor system or semiconductor-semiconductor system [12-14].

In this work, we will study the heterojunction between two semiconductors. To understand how a semiconductor device operates, it is essential to know the band lineup at the junction. The heterojunction between two semiconductors can divided into three types according to the band lineup of the two semiconductors.

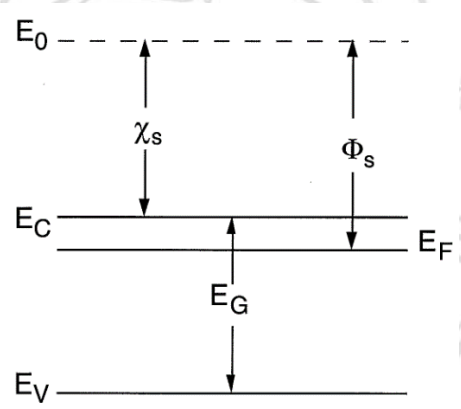

Fig. 1.6 Energy band diagram for a uniform semiconductor. The location of the conduction band is measured with respect to a reference energy level, E_0, the field-free vacuum level [11].

Considering the energy band diagram in Fig. 1.6, the work function (Φ_S), the position of conduction band energy level (E_C) and valence band energy level (E_V) are determined by the chemical bonding of atoms and can be calculated by solving Schrodinger's equation. These energy levels must be measured relative to reference level which is the vacuum level (E_0) in this figure. The E_0 is the energy of a free electron just outside the neutral semiconductor. The electron affinity (χ_S) is the energy needed to remove an electron from conduction band to make it free electron. The work function (Φ_S) of the semiconductor is defined as the energy required to take an electron from the Femi level through the bulk surface to the energy level of free space (or vacuum level) outside the

material. The work function, which depends on the Femi level, varies as a function of the doping level.

1.11.1 Heterojunction types [15]

Type I heterojunction: for example, the $Al_{0.3}Ga_{0.7}As/GaAs$ heterojunction shows that the conduction band and valence band of smaller band gap semiconductor lie completely within the band gap of wider band gap semiconductor.

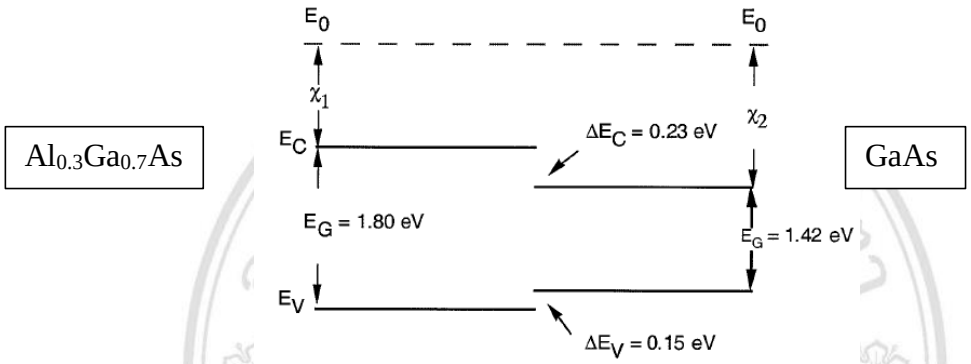

Fig. 1.7 Band alignment of type I heterojunction of $Al_{0.3}Ga_{0.7}As/GaAs$ [15].

From the band alignment between $Al_{0.3}Ga_{0.7}As$ and GaAs in Fig. 1.7, the conduction band difference can be calculated using Eq. 1.9.

$$\Delta E_C = \chi_2 - \chi_1 \quad (1.9)$$

where χ_2 and χ_1 refer to electron affinity of GaAs and $Al_{0.3}Ga_{0.7}As$, respectively.
In this kind of heterojunctions, the band gap energy is determined by using Eq. 1.10.;

$$\Delta E_G = \Delta E_C + \Delta E_V \quad (1.10)$$

Type II heterojunction: this can be found when the electron affinity difference between the two coupling materials are small. The conduction band of the smaller band gap semiconductor straddles the valence band of the larger band gap semiconductor such as $Al_{0.3}In_{0.7}As$ /InO system.

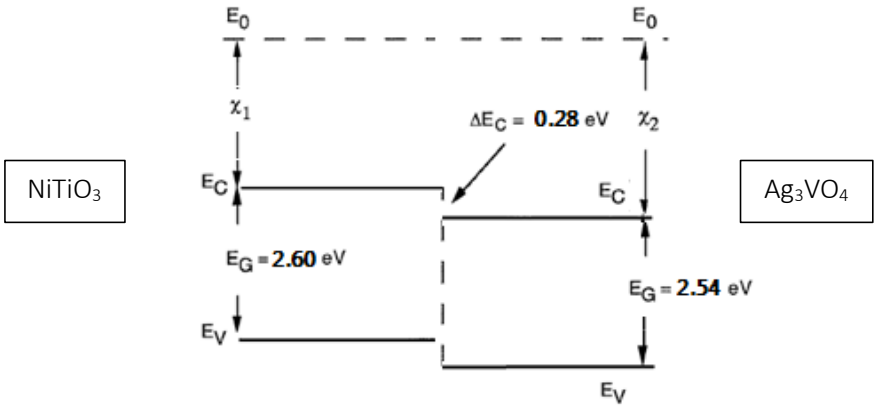

Fig. 1.8 Band alignment of type II heterojunction of $NiTiO_3/Ag_3VO_4$ conjunction [modified from 15,49].

Type III heterojunction: the conduction band of one semiconductor lies below the valence band of the other such as GaSb/InAs system (Fig. 1.9)

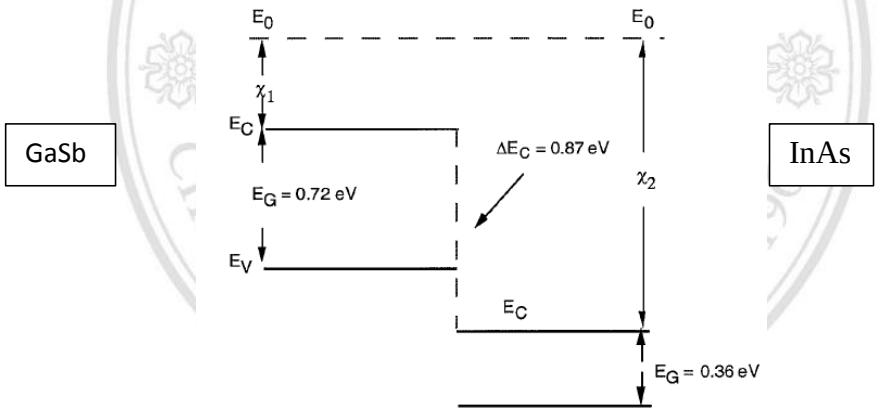

Fig. 1.9 Band alignment of type III heterojunction of GaSb/InAs [15].

1.12 The effect of band edge on pH of electrolyte solution [16]

The band edge position of semiconductor will normally depend on surface charging. This will be highly dependent not only on the ionic condition in a concrete electrolyte (pH, specific adsorption of ions), but also on the surface structure and composition of materials which depend on the particular synthetic strategy.

Owing to contact between the surface of semiconductor and electrolyte, the thermodynamic equilibrium in both sides of the interface must be established. In other words, the Femi level of semiconductor (E_F) is adjusted to the Femi level of the electrolyte ($E_{F,Redox}$). This equilibrium happens through electron transfer across the interface which results in the formation of space-charge layer called the "depletion

layer". For example, in the n-type semiconductor, the interface charge-transfer produces an excess of positive charges in the semiconductor and excess of negative charge in the electrolyte. With more electron exchanges, the electric field of the negative charges on the solution side hinders further electron transfer so that the equilibrium is established leading to no net charge flow. As a consequence, the bands are bent upwards which can be understood in term of a continuously growing barrier for interfacial electron transfer due to the positive charge in the depletion layer with less negative charge detection in the solution. The height of the barrier is the energy difference between the conduction band edge in the bulk semiconductor (E_C) and the conduction band edge at the surface ($E_{C,S}$) and corresponds to the potential drop in the space-charge layer, U_S as shown in Fig. 1.10

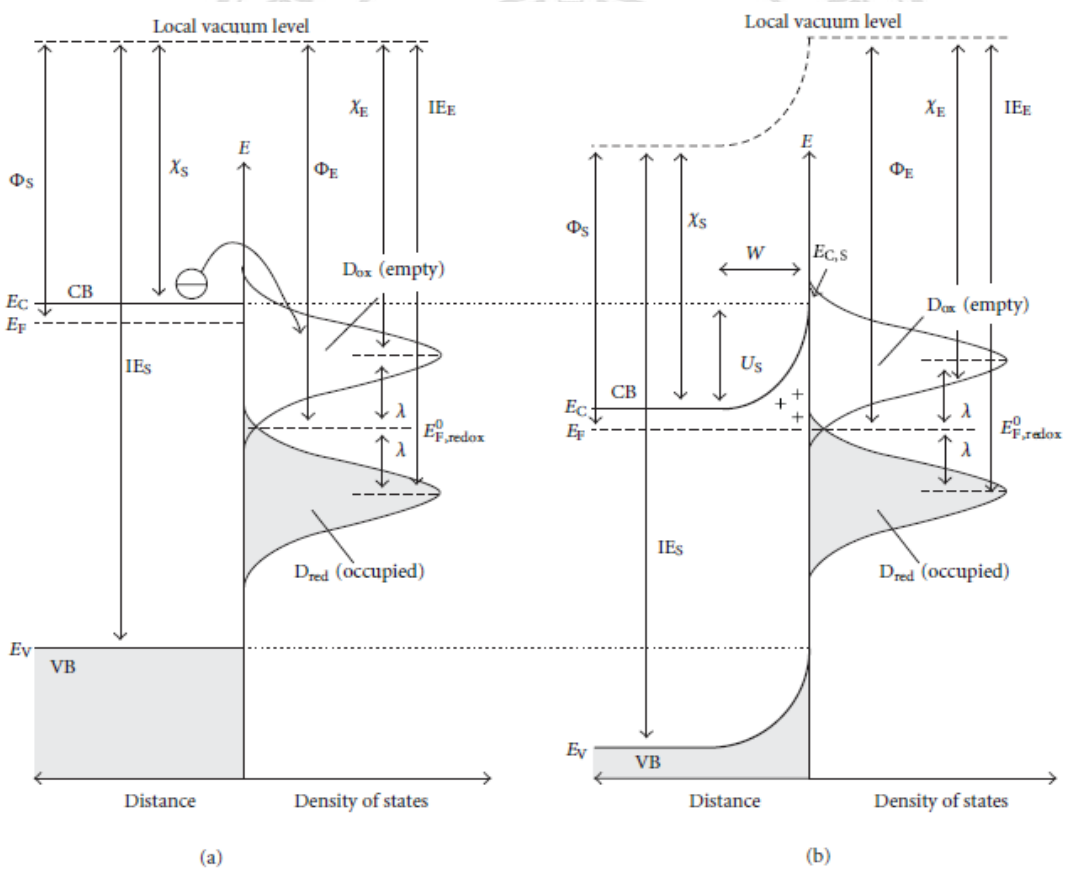

Fig. 1.10 Schematic energy model of the n-type semiconductor/electrolyte interface before (a) and after (b) the establishment of equilibrium. D_{red} and D_{ox} correspond to the distribution functions of the density of states for reduced and oxidized species, respectively. λ is the reorganization energy. Φ, χ, and IE are the work function, electron

affinity, and ionization energy, respectively, of the semiconductor (S) and of the electrolyte (E) [16].

The three distinct double layer at semiconductor/electrolyte interface can be distinguished. First, it is the semiconductor space-charge layer with positive charge in the form of ionized donors and the counter negative charge located at the surface. The second is the Helmholtz double layer consisting of the inner Helmholtz (IHP) and the outer Helmholtz plane (OHP). The first is located at the semiconductor surface and the charge is in the surface states, while the latter is closed to the hydrated mobile ions. Finally, there is a Gouy-Chapman layer where an excess of one sign free ions is presented as shown in Fig. 1.11.

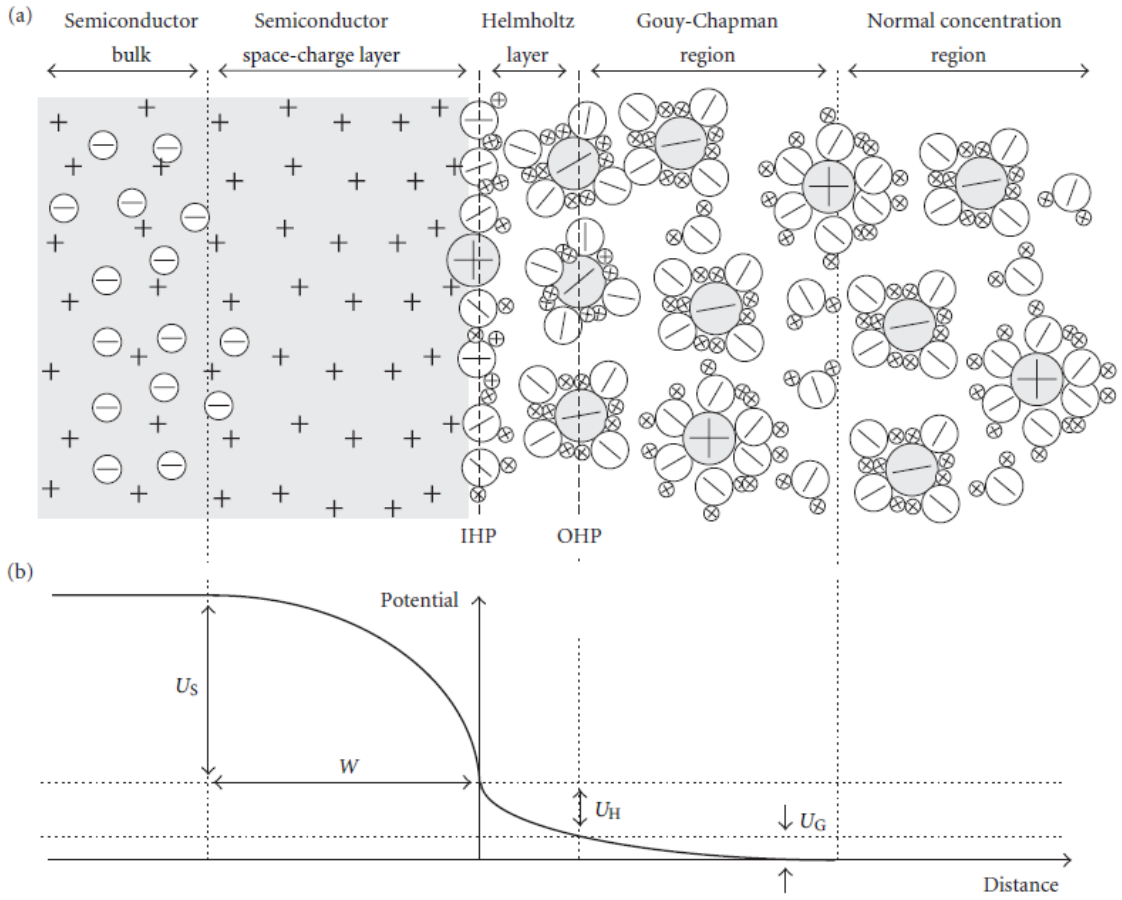

Fig. 1.11 Schematic view of the electric double layers at the n-type semiconductor/aqueous electrolyte interface (a) with corresponding potential distributions (b). U_S is the potential drop across the space-charge layer, U_H is the

potential drop in the Helmholtz layer, and U_G represents the drop in the Gouy-Chapman layer [16].

The position of band edge at the surface ($E_{C,S}$) is determined by the potential drop in the Helmholtz layer (U_H) as in Eq. 1.11:

$$E_{C,S} = E°_{C,S} - qU_H \quad (1.11)$$

where $E^0_{C,S}$ is the position (on the energy scale) of the conduction band edge at the surface at $U_H = 0$. The Helmholtz double layer at semiconductors is typically determined through adsorption and desorption processes which is particularly true for ionic oxide semiconductors like TiO_2 in aqueous electrolytes.

In this case, the protons and hydroxyl groups play an essential role while the specific adsorption of other ions can be in most cases neglected. The lattice Ti atoms act as Lewis acid sites and make the adsorption of hydroxyl ions possible, whereas the bridging lattice oxygen attracts protons and acts thereby as a Lewis base site. Hence, depending on the pH, the semiconductor surface becomes charged either positively or negatively (Fig. 1.12).

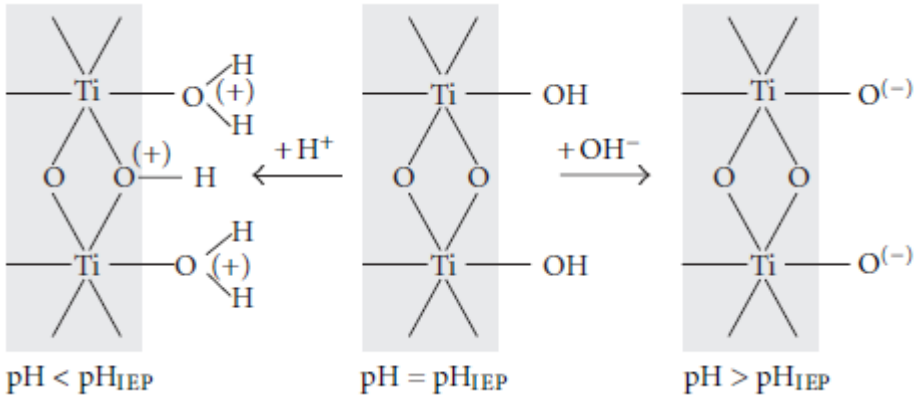

Fig. 1.12 Simplified scheme of the protonation and deprotonation of hydroxylated TiO_2 surface leading to positive and negative net charge at the surface, respectively [16].

The pH value at which the net surface charge is zero is called the isoelectric point (pH_{IEP}) or the point of zero zeta potential (pzzp). (It should be noted that pH_{IEP} and pzzp are not necessarily identical with the point of zero charge (pzc) that denotes the pH value at which H^+ and OH^- are adsorbed in equal amounts. When other ions are present and influence the charging of the surface, the pzc and the pH_{IEP} are not equal. The pH

dependence of the conduction band edge at the surface can be then derived as follows. Assuming pH < pH_{IEP}, we obtain the following equilibrium reaction (Eq. 1.12):

$$H_3O^+ \Leftrightarrow H_S^+ + H_2O \tag{1.12}$$

where H_3O^+ is a hydroxonium ion in the solution and H_S^+ is an adsorbed proton.

The equilibrium is described in Eq. 1.13.

$$\frac{[H_S^+]}{[H_3O^+]} = \exp\left(-\frac{\Delta G}{kT}\right) = A\exp\left(\frac{-qU_H}{kT}\right) \tag{1.13}$$

where ΔG is the Gibbs free energy, U_H is the potential drop in the Helmholtz double layer, and A is a constant (assuming that ΔG varies linearly with U_H). Assuming $[H_3O^+] >> [H_S^+]$, the following relation can be obtained (Eq. 1.14):

$$qU_H = B + kT \ln [H_3O^+] = B - 2.3kT\,pH \tag{1.14}$$

where $B = 2.3kT\,(pH_{IEP})$ assuming $U_H = 0$ at pH_{IEP}. By combining (1.11) and (1.14), we obtain (Eq. 1.15):

$$E_{C,S} = E^0_{C,S} + 2.3kT\,(pH - pH_{IEP}) \tag{1.15}$$

Accordingly, with increasing pH, the band edges at the surface shift to higher energies (on the energy scale), that is more cathodic potentials (on the electrode potential scale), whereby the shift at 298 K is typically $\sim$0.059 V/pH unit.

1.13 Theoretical predictions of the position of band edges: **[16]**

Butler and Ginley introduced a theoretical approach for the prediction of the position of band edges using the following relation (Eq. 1.16):

$$E_{C,S} = X - E^e - 1/2E_g \tag{1.16}$$

where E^e is the energy of free electrons on the hydrogen scale (4.44 ± 0.02 eV), E_g is the band gap energy, and X is the Sanderson electronegativity of the semiconductor, expressed as the geometric mean of the electronegativities of the constituent atoms which are defined after Mulliken as the arithmetic mean of the atomic electron affinity and the first ionization energy (both in eV unit). Calculation for TiO_2 gives X = 5.8 eV

which (assuming $1/2E_g$ = 1.6 eV for anatase) yields the $E^0_{C,S}$ value of -0.24 eV vs NHE.

1.14 Organic pollutant [4, 17-19]

In this research, we are interested in studying the degradation of methylene blue. Methylene blue is a cationic dye. It is commonly used for coloring paper, temporary hair colorant and dyeing cotton wools. Although, methylene blue is not considered to be a very toxic dye, it can create harmful effects on the creatures, such as difficulties in breathing, vomiting, diarrhea and nausea. The molecular formula of methylene blue is $C_{16}H_{18}N_3SCl$. Its IUPAC name is 3,7-bis(dimethylamino)-phenothiazin-5-ium chloride. The structural formula is shown in Fig. 1.13.

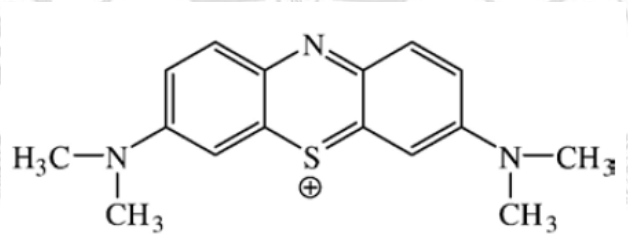

Fig. 1.13 Structure of methylene blue [3].

The visible light absorption spectra (Fig. 1.14) of diluted methylene blue solution contain the band at 665 nm due to $\pi \rightarrow \pi^*$ transition. A small shoulder at shorter wavelength about 608 nm is related to dipole-diplole interaction between the methylene blue monomer components in the aggregate to present the dimeric species [20].

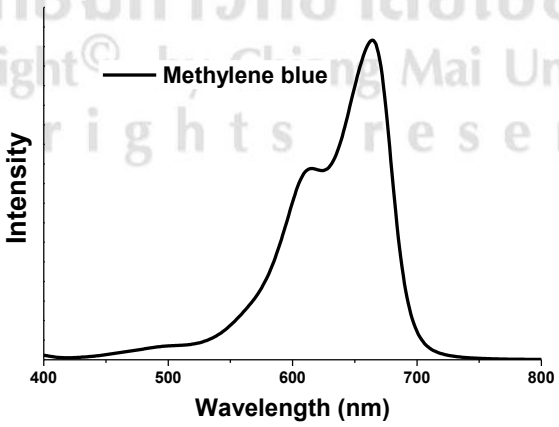

Fig. 1.14 Absorption spectra of methylene blue [modified from 20].

As international environmental standards are becoming more stringent (ISO 14001, October 1996), technological systems for the removal of organic pollutants, such as dyes have been intensively investigated. Among them, physical methods (adsorption), biological methods (biodegradation) and chemical methods (chlorination, ozonation) are the most frequently used. However, the new oxidation methods or advanced oxidation processes (AOP) based on heterogeneous photocatalysis recently appears as an emerging destructive technology leading to the total mineralization of most of the organic pollutants. The usually proposed mechanism for photocatalytic degradation of organic compounds over the well-known TiO_2 photocatalyst is shown below.

1. Absorption of efficient photons ($h\nu \geq E_g = 3.2$ eV) by TiO_2

$$TiO_2 + h\nu \rightarrow e^-_{CB} + h^+_{VB}$$

2. Oxygen ionosorption (first step of oxygen reduction; oxygen's oxidation number passes from 0 to −1/2)

$$(O_2)_{ads} + e^-_{CB} \rightarrow O_2^{\circ -}$$

3. Neutralization of OH− groups by photogenerated holes which produces OH◦ radicals

$$(H_2O \Leftrightarrow H^+ + OH^-)_{ads} + h^+_{VB} \rightarrow H^+ + OH^\circ$$

4. Neutralization of $O_2^{\circ}-$ by protons

$$O_2^{\circ -} + H^+ \rightarrow HO_2^\circ$$

5. Transient hydrogen peroxide formation and dismutation of oxygen

$$2HO_2^{\circ -} \rightarrow H_2O_2 + O_2$$

6. Decomposition of H_2O_2 and second reduction of oxygen

$$H_2O_2 + e^- \rightarrow OH^\circ + OH^-$$

7. Oxidation of the organic reactant via successive attacks by OH◦ radicals

$$R + OH^\circ \rightarrow R^\circ + H_2O$$

8. Direct oxidation by reaction with holes

$$R + h^+ \rightarrow R^{+\circ} \rightarrow \text{degradation products}$$

As an example of the last process, holes can react directly with carboxylic acids to generate CO_2 and H_2O as final products.

$$RCOOH + h^{+} \rightarrow H_2O + CO_2$$

1.15 Synthesis methods for semiconductor photocatalysts

1.161.15.1 Sol-gel method [21]

The sol-gel method is usually used to prepare various novel ceramic oxides with controlling size and morphology such as TiO_2, $BaTiO_3$, CeO_2 and Fe_3O_4. The advantages of this method are higher purity, better homogeneity and lower processing temperature compared with the traditional ceramic powder method.

'Sol' is a dispersion of colloid particles in a liquid phase. These colloid particles have a diameter in the range of 1-100 nm.

'Gel' is a rigid three dimension network with well ordering lamellar or polymer chain that its length is longer than a micrometer.

From the review of Larry et al. [21] on the sol-gel synthesis of SiO_2, there are seven steps involving the method.

Step 1: mixing step

The sol is formed in this step by mixing all precursors together. The liquid alkoxide precursors are such as $Si(OR)_4$ where R is CH_3, C_2H_5 or C_4H_9. The alkoxide complex is hydrolyzed by nucleophile (OH^-). The silanol bonds (Si–OH) are formed as mechanism below.

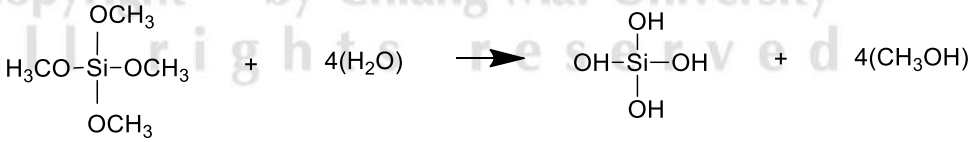

The hydrated molecules reacts with each other in polycondensation reaction, thus SiO_2 network is formed via Si-O-Si linkage. The water is released from the reaction, resulting in a pore in the network.

Step 2: Casting step

The low viscosity of polymerized network is casted into the mold.

Step 3: Gelation step

The silica species are linked together to become three dimensional network as shown below. At gelation point, the viscosity is significantly increased and silica species turn into the rigid solid.

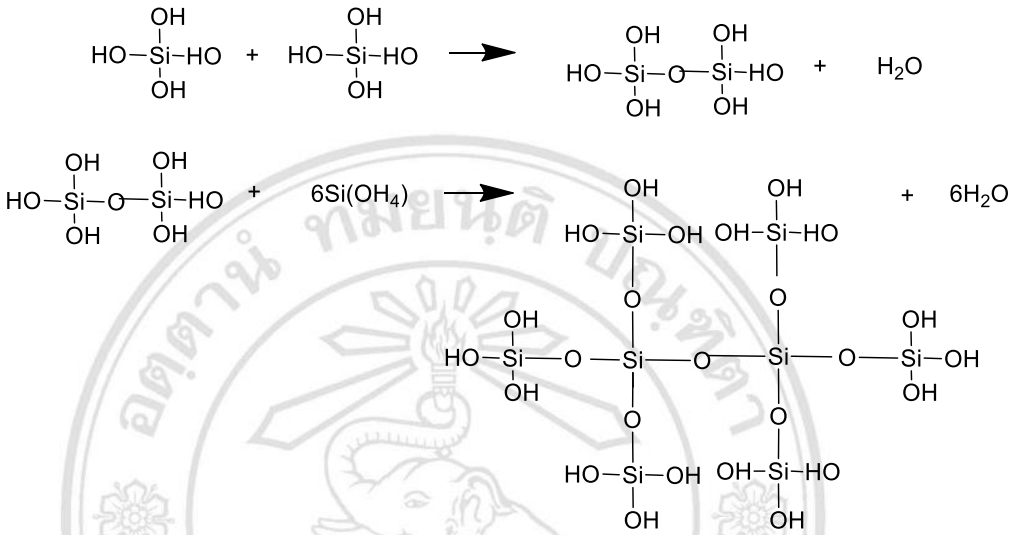

Step 4: Aging step or syneresis step

Increasing the thickness of three dimensional network and porosity generation are appeared. An aged gel improves the strength of silica dimension in order to protect cracking of the gel network during drying.

Step 5: Drying step

The liquid that penetrate into the gel network was evaporated by heating. In this process, the small pores are developed, so the aerogel (porous network after expelling the liquid) attains low density.

Step 6: Dehydration or Chemical stabilization

The polycondensation process is stopped by removing the surface silanol groups (Si-OH) from silica network leading to a release of water and a formation of chemical stable molecule.

Step 7: Densification

Heating the porous gel with high temperature, the pores are eliminated and the network is collapsed. Densification process increases density of silica

monoliths and eliminates the organic residue from the network, so the metal oxide powder is obtained.

1.15.2 Hydrothermal processes [6,22]

Water is an excellent solvent for many ionic compounds (salt). At high pressure and temperature far above its boiling point at 1 bar pressure (hydrothermal conditions), it can also dissolve nonionic covalent compounds such as insoluble metal oxides. In this case, water serves two different functions as both solvent and the pressure transmitting medium. Furthermore, many inorganic phases which are unstable under traditional high temperature, solid state synthesis condition, can be synthesized by hydrothermal process to avoid the severe conditions.

However, the solvent properties of pure water are often not sufficient to dissolve substances for crystallization even at high temperature, so it is necessary to add a mineralizer. A mineralizer is any compound added to the aqueous solution to speed up crystallization. It usually operates by increasing the solubility of the solute through the formation of soluble species that would not normally be present in the water. Typical mineralizers are the hydroxides of the alkali metals such as NaOH, and KOH.

For most hydrothermal syntheses, only moderate temperatures (100-300 °C) at the corresponding low solution vapor pressures (subcritical region) are applied. The nutrient solution usually consisting of oxides, hydroxides, and salts of the corresponding metal is fed into the autoclave. This solution is heated and at the desired reaction temperature the nutrient materials react and transform, primarily through dissolution and precipitation to the stable compound. After cooling the autoclave, the product can be isolated by filtration, following by a series of washing steps to obtain the pure product.
The autoclave for a hydrothermal reactor is a thick-walled steel reactor able to sustain high pressures at elevated temperatures. Powders dissolve in the lower and hotter part of the reactor and crystallize in the form of single crystals in the upper part.

Many oxidic gem stones have been formed hydrothermally in inorganic nature and it is not difficult to grow rather large single crystal of oxides using hydrothermal process. Single crystals of quartz are made hydrothermally in industry to get a low growth

temperature. Not only single crystals but also powders are made hydrothermally on an industrial scale, e.g., zeolites, apatites, and ceramic precursors.

1.15.3 Precipitation process [22]

In precipitation processes, water is mostly used as a solvent. Precipitation is the process in which a precipitate is formed from two solution salt corresponding to the constituent ions of the product. The initial formation of particles from solution proceeds as indicated in Fig. 1.15.

The concentration of the solute is continuously increased up to the minimum concentration for nucleation, C_0. No precipitation takes place at this stage.

When C_0 is reached, nucleation sets in. The concentration of solute increases to the maximum concentration for nucleation, C_N, and then decreases again due to the consumption of the solute by nucleation and precipitation of particles. The range between C_S and C_N corresponds to a supersaturation. At the critical concentration, C_N, nucleation is very rapid.

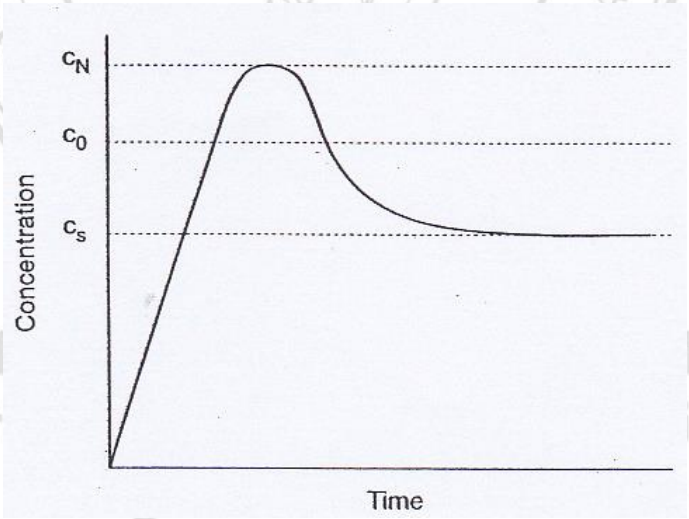

Fig. 1.15 Concentration of the solute before and after nucleation. [22].

Once the minimum concentration for nucleation, C_0, is reached again, new nuclei are no longer formed. Crystal growth reduces the concentration until the equilibrium solubility, C_S, is reached.

Separation between the nucleation and the growth state is the primary requirement for obtaining uniform particles. This means that after nucleation, the particle-forming solute

species must continue to be formed at certain rate that allows their removal from solution by reaction with the existing particles so that no secondary nucleation can take place. The rate of growth of the particles may be controlled by diffusion of dissolved species to the particle or by the rate of the condensation reactions between the particle and dissolved species.

An alternative supply of particle-forming species is by dissolution of small particles. The smaller particles are more soluble than larger particles due to the curvature effects. Thus larger particles grow at the expense of smaller ones. Larger, more stable particles are formed by a process called 'Ostwald ripening'. Moreover, a nucleation-aggregation model was proposed for such cases that assume the initial small primary particles to be too unstable owing to their small size. They aggregate to secondary particles and freshly formed primary particles attach to the aggregates. Monodispersity of the final precipitate is achieved through size-dependent aggregation rates. The aggregate structure apparently causes a collective reduction in surface area. The concomitant reduction in surface energy is the driving force for the ordered aggregation.

Particles form by this process should be crystalline, although amorphous, porous particles are frequently obtained. Crystal growth is only possible if the attachment of the molecular species is weak enough allowing the species to redissolve and attach to the surface in a position required for a crystalline structure. This is more likely in dilute solutions.

1.16 Literature Reviews

1.16.1 Silver vanadate structure [23-27]

Silver vanadate (Ag_3VO_4) is mainly found in three polymorphs which are α-Ag_3VO_4, β-Ag_3VO_4 and γ-Ag_3VO_4. In all three polymorphs, both silver and vanadium cations are 4-fold coordinated by oxygen. At room temperature, α-phase is a stable polymorph; whereas β-phase and γ-phase are stable in the temperature range of 110 °C-414 °C and 414 °C-530 °C, respectively. Due to the low stability of β-Ag_3VO_4 and γ-Ag_3VO_4 phases, the characterization on physicochemical properties of the materials has only been performed by in situ X-ray diffraction above the phase transition temperature. The polycrystalline data of three polymorphs are shown in Table 1.3. The *α*-phase has a monoclinic structure (space group C2/*c*) with band gap energy of about 2.4 eV, whereas

the β-phase is the tetragonal famatinite structure (space group $I\bar{4}2m$) with band gap energy of 2.67 eV. The γ-phase belongs to the cubic crystal structure (space group $F\bar{4}3m$), but was not further investigated due to its unstabilized phase.

Structural Ag_3VO_4 was described by Belver et al. [24] as a distorted anti-sphalerite type monoclinic structure. It was found as a cubic closest-packed arrangement of metal cations with the O^{2-} filling half of the tetrahedral positions. Thus, Ag^+ exhibits two different coordination spheres, distorted square planar and pseudo-see-saw arrangement, while vanadium is tetrahedrally coordinated to four oxide anions as shown in Fig. 1.16.

Table 1.3 Comparison on the main characteristic features between α-phase and β-phase of Ag_3VO_4 [23].

Features	**α- Ag_3VO_4 phase**	**β- Ag_3VO_4 phase**
Crystal system	monoclinic	Tetragonal
Space group	C2/*c*	$I\bar{4}2m$
Cell parameters		
a (Å)	10.1759	4.9795
b (Å)	4.9784	4.9795
c (Å)	10.2142	9.7270
V (Å^3)	466.31	241.19
ρ (g/cm^3)	6.247	6.039

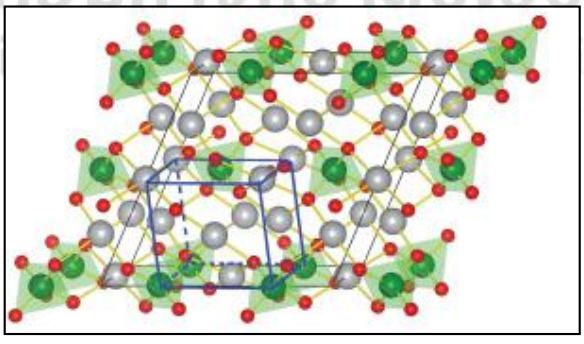

Fig. 1.16 Structure of monoclinic α-Ag_3VO_4 where the gray, green and red atoms refer to silver, vanadium and oxygen, respectively [25].

Ag_3VO_4 has been proven to be a good visible-light responsive photocatalysts, especially in the field of photocatalytic splitting of water into H_2 and O_2. The valence band of Ag_3VO_4 consists of hybridized Ag $4d^{10}$ orbital and O_2p^6 orbital, while the conduction band consists of hybridized Ag 5s orbitals and V 3d orbitals. For the Ag containing photocatalysts, the hybridization of the O_2p^6 orbitals with the completely filled $4d^{10}$ orbitals of silver ion could form a valence band at more positive energy level than that of O_2p^6 resulting in a narrow band gap energy.

The Ag_3VO_4 can produce O_2 evolution from aqueous silver nitrate solution under visible light irradiation. This indicates that the valence band level is more positive than the O_2/H_2O reduction half-cell potential energy (1.23 V vs. SHE, pH 0). Therefore, a strong oxidizing potential of Ag_3VO_4 could benefit high degradation of organic compounds.

A summary of synthesis method in Table 1.4 suggests that Ag_3VO_4 is usually prepared by precipitation and hydrothermal method. As discussed previously, that the efficient transfer of electron-hole pairs in coupling system between two semiconductors is needed for strong chemisorption interaction. This strong interaction in composite can be efficiently attained by using the hydrothermal method where the reaction is performed under high pressure and high temperature. Although, the precipitation method is an easier method to obtain the powder at room temperature (RT), this gentle condition may provide the coupling material with weak interaction. Therefore, the hydrothermal method will be used in this study to synthesize both pure Ag_3VO_4 powders and the composite between $Ag_3VO_4/CoTiO_3$ in various weight ratios.

1.16.2 Synthesis methods for Ag_3VO_4

Table 1.4 A summary of synthesis methods for Ag_3VO_4.

No.	Methods	Precursors	Optimized conditions	Phase purity
1 [28]	Precipitation	$NaVO_3$ and $AgNO_3$	1.Aged 24 h at RT	Pure Ag_3VO_4
2 [29]	Precipitation	NH_4VO_3 and $AgNO_3$	1.Aged 24 h at RT, pH 14	Pure Ag_3VO_4
3 [27]	Hydrothermal	$NaVO_3$, NH_4VO_3 and $AgNO_3$	1.Heated at 160 °C for 48 h, pH 7	Pure Ag_3VO_4
4 [30]	Hydrothermal	NH_4VO_3 and $AgNO_3$	1.Heated 140 °C for 4 h, pH 7	Pure Ag_3VO_4
5 [31]	Hydrothermal	$NaVO_3$ and $AgNO_3$	1.Aged 24 h at RT, pH 7 2.Heated at 140 °C for 4 h	Ag_3VO_4 and $Ag_4V_2O_7$
6 [32]	Hydrothermal	$NaVO_3$ and $AgNO_3$	1.Aged 24 h at RT, pH 7 2.Heated 140 °C for 6 h	Pure Ag_3VO_4

1.16.3 Cobalt titanate structure [33-35]

The corundum-type structure of A_2O_3 sesquioxides (oxides that contain cation atoms to anion atoms in a 2:3 ratio) basically consists of a hexagonal closest-packed array of oxide ions, with trivalent A cations occupying two-thirds of the octahedral holes. This structure belongs to the $R\bar{3}c = D_{3d}^6$ space group. The two different cation ordering can occur when half of the A cations of the corundum-type sesquioxide are substituted by B cations, giving an ABO_3 hexagonal mixed oxide. Obviously, A and B cations can be both trivalent or divalent A and tetravalent B (as an ilmenite-type structure) or monovalent A and pentavalent B. The disappearance of three glide planes with retension of the center of symmetry and the trigonal axis gives lower symmetry of $R3c = C_{3v}^6$ space group.

$CoTiO_3$ has an Ilmenite-type structure in which Co^{2+} and Ti^{4+} form alternating layer along rhombohedral axis of the crystal with oxygen layer between them. From Fig. 1.17, the oxygen ions have the approximately hexagonal close-packing along the c-axis and cations occupy two-thirds of the octahedral interstices [36].

In such a structure, Ti and Co atoms form pairs separated by a vacant site along the rhombohedral axis. As a consequence, a metal-metal interaction is allowed between the d orbitals (of t_2g symmetry) extending their lobes through the face shared by the two octahedra.

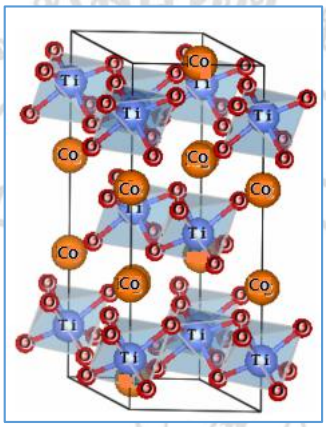

Fig. 1.17 Structure of Ilmenite $CoTiO_3$ [modified from 37].

1.16.4 Synthesis methods for $CoTiO_3$

Table 1.5 A summary of synthesis methods of $CoTiO_3$.

No.	Methods	Precursors	Optimized conditions	Phase purity
1 [38]	Sol gel	Cobalt acetate, Titanium isopropoxide, 2-methoxy ethanol	1.Stir at RT for 12 h 2.Calcine at 150 °C for 1 h 3.Calcine at 550 °C for 2 h	Pure $CoTiO_3$
2 [39]	Sol gel	Cobalt chloride, Titanium isopropoxide, Citric acid Acetylacetone	1.Dry at gel at 200 °C for 1 h 2.Calcine at 800 °C for 1 h	$CoTiO_3$ and rutile of TiO_2
3 [40]	Sol gel	Cobalt acetate, Titanium n-butoxide, Ethylene glycol	1.Stir at 170 °C for 3 h 2.Dry at 80 °C for 6 h 3.Heat at 800 °C for 6 h	Pure $CoTiO_3$

Table 1.5 A summary of synthesis methods of $CoTiO_3$ (continued).

No.	Methods	Precursors	Optimized conditions	Phase purity
4 [41]	Sol gel	Cobalt nitrate hexahydrate, Titanium dioxide P-25, Cetyltrimethylammonium (CTAB), Sodium hydroxide	1.Reflux at 75 °C for 12 h 2.Dry at 100 °C for 12 h 3.Calcine at 600 °C for 6 h	$CoTiO_3$ and rutile of TiO_2
5 [42]	Precipitation	Titanium tetrachloride, Cobalt nitrate hexahydrate, Hydrochloric acid, Urea	1.Dry at 130 °C for 24 h 2.Calcine at 800 °C for 6 h	$CoTiO_3$ and rutile of TiO_2
6 [43]	Pechini	Cobalt acetate, Tetrabutyl titanate, Ethylene glycol, Citric acid monohydrate	1.Dry at 130 °C for 8 h 2.2 step heated at: 600 °C for 3 h 800 °C for 6 h	Pure $CoTiO_3$
7 [44]	Sol gel	Titanium (IV) n-butoxide, Cobalt acetate, Stearic acid as complexing agent	1.Dry 12h (gel) 2.Calcine at 400 °C for 40 mins (1^{st} step) Calcine 600 °C for 2 h (2^{nd}step)	$CoTiO_3$ and Co_3O_4

From Table 1.5, most synthesis method used for $CoTiO_3$ is sol gel method which can provide the pure phase under mild condition. Moreover, the method can also produce materials with small particle size and high surface area; therefore, the sol gel method is used to synthesize $CoTiO_3$ powder in this research.

1.16.5 Composites [7]

Simple materials or solid compounds are combined into one composite for several reasons:

1. The desirable properties of a material can be improved upon composite formation.

2. At the same time, the unwanted characteristics of the components can in many cases be neutralized or eliminated in the composite.
3. Novel properties that do not exist in the simple materials can be created and apparently conflicting properties can be combined in one composite.

For example, a ceramic hard coating on a metal substrate gives a hard, wear-resistant, and corrosion-resistant product that is also strong and tough. It combines the good bulk and surface properties of the components and eliminates their less desirable characteristic which is the synergistic effects in composites.

Properties of composites can be more easily adjusted than those of simple solid compounds because the behavior of composites depends on how much each component contributes and how the components are made to cooperate in the composite.

1.16.6 Reviews on the enhanced coupling system (composites)

Nowadays, the public is increasingly concerned about the environmental issues. One of major environmental problems is waste water which is considerable to be hard for elimination. Regarding to this problem, a degradation of organic contaminants via photocatalysis is extensively studied as a viable mean to help solve the problem. TiO_2 is the most widely used photocatalyst due to its high efficiency for organic molecule degradation. Although TiO_2 catalyst has high activity and high chemical stability, it can be activated only by UV light because of its wide band gap energy (3.2 eV), thus only 4% of natural solar light can be absorbed by TiO_2 [45]. Therefore, visible-light-driven photocatalyst is investigated to enhance the photoactivity.

Silver vanadate is one of the effective candidate visible light-driven photocatalyst (band gap energy of about 2.2-2.4 eV). Various structures of silver vanadate such as α-$AgVO_3$, β-$AgVO_3$, $Ag_4V_2O_7$ and Ag_3VO_4 have been found, but only Ag_3VO_4 is reported to exhibit a photocatalytic activity [28]. Ag_3VO_4 has over 3 times higher activity than TiO_2 that can be used to degrade the dangerous volatile organic compound, i.e. isopropanol, benzene and phenol. Moreover, the surface of Ag_3VO_4 contains high amount of surface hydroxyl group which can increase a degradation rate. However, practical application of the Ag_3VO_4 is still inhibited by its high electron–hole recombination rate due to its intrinsic narrow band gap energy [30, 32]. Therefore,

modification of this catalyst is needed. The widely used methods for improving the efficiency of photocatalysts are doping metal or non-metal species into host material, and forming a composite between a suitable sensitizer and host material [46]. However, metal doping sometimes causes the defect sites where the electron–hole recombination is generally occurred [47]. Therefore, the preferable way to modify photocatalyst is to composite the host material with an appropriate sensitizer.

Composite materials have been studied intensively in the past few years, and the enhanced photoactivity of the composites are ascribed to the suitably matching of conduction band and valence band for an effective charge transfer across the coupled semiconductors. As mentioned previously that only the type II heterojunction is able to enhance the photocatalytic activity. Therefore, much effort has been paid to obtain this type of heterojunction as summarized below.

Co_3O_4/Ag_3VO_4 composite has firstly been studied by Zhang *et al.* [48]. Therein, the Ag_3VO_4 photocatalyst is modified with Co_3O_4 via impregnation technique. Upon increasing Co_3O_4 content, an increased specific surface area and a red shift in band energy are found. The photocatalytic activity test of RhB degradation shows the best activity from the 0.1% Co_3O_4/Ag_3VO_4. The charge transfer mechanism in Fig. 1.18 indicates that electrons from the CB of Ag_3VO_4 are transferred to that of Co_3O_4; whereas, holes at the VB of Co_3O_4 are transferred to that of Ag_3VO_4. This electron–hole pair can participate in the production of active species; therefore, Co_3O_4 helps improve the photocatalytic activity of Ag_3VO_4.

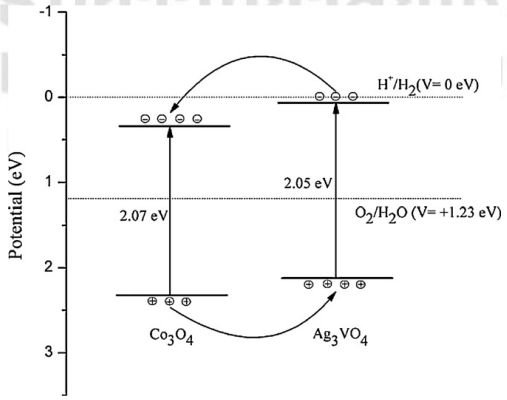

Fig. 1.18 Schematic diagram of synergistic effect of Co_3O_4/Ag_3VO_4 [48].

By loading NiO onto Ag_3VO_4 surface to trap electron from a light exciting process, an improved photocatalytic activity of 3.8 times higher than that of Ag_3VO_4 is found from

NiO/Ag_3VO_4 composite [30]. Due to no activity of NiO, excess NiO particle might decrease the light absorption ability. The NiO/Ag_3VO_4 photocatalyst produces $O_2^{\bullet-}$ on the surface, and decolorizes azodye acid red B (ARB) within 100 minutes. The presence of active radical indicates that NiO/Ag_3VO_4 can generate electron–hole pairs, and decompose dye pollutants. Coupling between TiO_2 and Ag_3VO_4 is also found to improve the solar energy utilization of TiO_2, and the separation of electron–hole pairs of Ag_3VO_4 at the same time [45]. The photocatalytic activity shows that 0.5% Ag_3VO_4 loading gives the highest activity with obviously enhanced ability of visible light absorption. The coupling material can improve electron generation capacity and electron transfer effectiveness which are detected by photoluminescence (PL) technique. The mechanism of photocatalytic process is shown in Fig. 1.19. When Ag_3VO_4 is activated by visible light (solid line), the electrons on the VB of Ag_3VO_4 is excited to CB and transferred to the CB of TiO_2 to react with O_2. The process in dash line happens when solar light is used as a light source. The hole on VB of TiO_2 can transfer to VB of Ag_3VO_4. From this hole transfer step, the hydroxyl radicals are generated directly by reacting with water molecules.

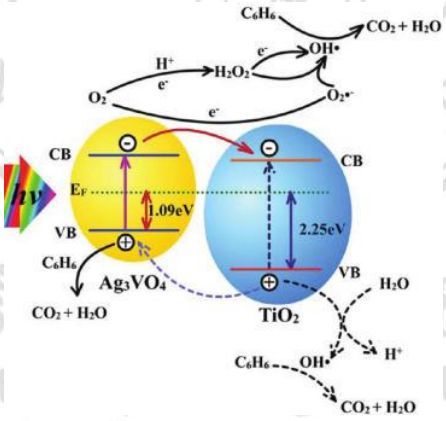

Fig. 1.19 Proposed degradation mechanism of Ag_3VO_4/TiO_2 system under visible light irradiation (solid line) and simulated solar light irradiation (solid line and dashed line) [45].

New $NiTiO_3/Ag_3VO_4$ [49] composite is also found to exhibit enhanced photoactivity under visible light stimulation. The light harvesting and separation of electron–hole pair properties of this photocatalyst are improved. Since the two semiconductors are bounded by chemical interfaces, an effective charge transfer between two matching energy levels is achieved. By this intimate contact, a long life-time of photogenerated

charge carriers is found according to PL experiment in Fig. 1.20 (a). The band position in Fig. 1.20 (b) is consistent with a type-II heterojunction. The electron from VB of both semiconductors is excited to CB, and the electron on the CB of $NiTiO_3$ is transferred to the CB of Ag_3VO_4 whereas the hole on the VB of Ag_3VO_4 is transferred to the VB of $NiTiO_3$ to produce active species.

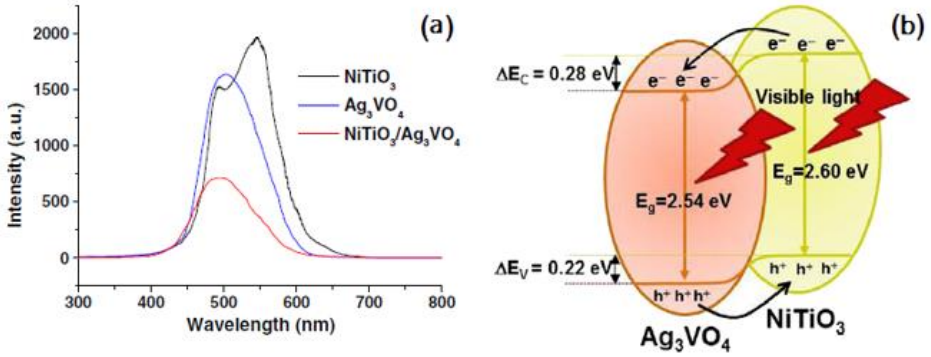

Fig. 1.20 (a) Comparison of PL spectra and (b) a proposed electron–hole transfer mechanism at the $NiTiO_3/Ag_3VO_4$ interface [49].

1.17 Aim and scope of this study

To enhance photocatalytic activity, the formation of heterojunction based on the concept of heterostructure charge separation is carried out in this work. Since the electron-hole pairs can be transferred between the coupling materials, longer life time of photogenerated charges, hence more active species being produced, could lead to the enhanced photocatalytic activity of the material [50]. Many reports have shown that the heterojunction formation between Ag_3VO_4 and other semiconductors could improve the photocatalytic activity such as Ag_3VO_4/TiO_2 [45], Ag_3VO_4/NiO [30], Ag_3VO_4/Co_3O_4 [48], $Ag_3VO_4/ZnFe_2O_4$ [51], Ag_3VO_4/g-C_3N_4 [52], Ag_3VO_4/Gd_2O_3 [53]. Therefore, forming a heterostructure photocatalyst has been chosen as an approach to improve the photoactivity of Ag_3VO_4. In this study, $CoTiO_3$ is selected to composite with Ag_3VO_4 due to its various beneficial properties to be a good photocatalytic material such as good stability in adverse environments, ability for oxygen evolution, easy preparation and narrow band gap energy and a visible-light response activity [54]. Moreover, various applications of $CoTiO_3$ are found such as gas sensor for Liquefied Petroleum Gas (LPG) detection, pigment for glasses, ceramics, and humidity sensor [55-58].

The $Ag_3VO_4/CoTiO_3$ composite materials will be characterized by X-ray diffractometry (XRD), scanning electron microscopy (SEM) and UV-vis diffuse reflectance spectroscopy (UV-vis DRS), etc. in order to obtain the characteristic features of these materials. The photocatalytic activity of the obtained material will be evaluated by UV-vis spectroscopy. The energy band alignment of this novel heterojunction system, which is determined from X-ray photoelectron spectroscopy (XPS) study, will also be proposed in order to better understand an improved photocatalytic efficiency of this new system. Additionally, the main active species driven photocatalytic activity of this system will be investigated and the main degradation mechanism will also be proposed. The role of each component in the $Ag_3VO_4/CoTiO_3$ composite will be examined by the experiments under different light activation wavelengths.

1.18 Usefulness of the research (Theoretical and/or Applied)

1.18.1 The composite obtained from this research will be a model compound showing that the improved photocatalytic activity can be attained based on the idea of suitably matching VB and CB levels.

1.18.2 The method of forming composite structures could also be used as an alternative approach to improve the activity of other composite-based photocatalytic materials. This will also be beneficial to the design of new and more efficient heterostructure-based photocatalysts.

REFERENCES

[1] B. Viswanathan, S. Sivasanker, A. V. Ramaswamy, *Catalysis Principles and Applications*, Narosa Publishing House, New Delhi Chennai, India, 2006.

[2] M. Fox, *Optical Properties of solids*: *oxford master series in condensed matter physics*, Oxford University Press, New York, 2006.

[3] W.H. Strehlow and E. L. Cook, *Journal of Physical Chemistry*, **2** (1973) 163.

[4] Q. Wang, S. Tian, and P. Ning, *Industrial and Engineering Chemistry Research*, **53** (2014) 643.

[5] Akihiko Kudo and Yugo Miseki, *Chemical Society Reviews*, **38** (2009) 253.

[6] P. J. V. D. Put, *The inorganic chemistry of materials*, Plenum Press, New York, 1998.

[7] V. Ponec, Z. Knor, and S. Cerny, Adsorption on solids, Butterworths group, Czechoslovakia, 1974.

[8] M. R. Wright, *An introduction to Chemical Kinetics*, John Wiley & Sons Ltd, England, 2004.

[9] H. Chang, C. Su, C.-H. Lo, L.-C. Chen, T.-T. Tsung, and C.-S. Jwo, *Materials Transactions*, **45** (2004) 3334.

[10] L. Pei, Z. Peng, C. D.-Liang, and X. W.-Ting, Chinese Science Bulletin, 57 (2012) 4381.

[11] A.G. Milnes and D. L. Feucht, *Heterojunctions and Metal-Semiconductor Junctions*, Academic Press, New York, 1972.

[12] F. Dong, Z. Zhao, T. Xiong, Z. Ni, W. Zhang, Y. Sun, and W.-K. Ho, *ACS Applied Materials and Interfaces*, **5** (2013) 11392.

[13] Y. Wang, R. Shi, J. Lin, and Y. Zhu, *Energy and Environmental Science*, **4** (2011) 2922.

[14] W. Liu, M. Wang, C. Xu, and S. Chen, *Chemical Engineering Journal*, **209** (2012) 386.

[15] M. Lundstrom, *Heterostructure Fundamentals*, School of Electrical and Computer Engineering and the NSF MRSEC for Technology-Enabling Heterostructures Purdue University, West Lafayette, Indiana, 1995.

[16] R. Beranek, *Advances in Physical Chemistry*, **2011** (2011) 20.

[17] T. Omata, K. Ono, and S. O.-Y.-Matsuo, *Materials Transactions*, **44** (2003) 1620.

[18] J. Bujdak, and P. Komadel, *Journal of Physical Chemistry B*, **101** (1997) 9065.
[19] N.P. Mohabansi, V.B. Patil, and N. Yenkie, *Rasayan J. Chem.*, **4** (2011) 814.

[20] A. Ghanadzadeh, A. Zeini, A. Kashef, and M. Moghadam, *Journal of Molecular Liquids* **138** (2008) 100.

[21] L. L. Hench and J. K. West, *Chemical Reviews*, **90** (1990) 33.

[22] U. Schubert, and N. Husing, *Synthesis of Inorganic Materials*, Wiley-VCH, Germany, 2000.

[23] V. Cloet , A. Raw , K. R. Poeppelmeier , G. Trimarchi , H. Peng , J. Im , A.J. Freeman , N. H. Perry , T. O. Mason , A. Zakutayev , P. F. Ndione , D. S. Ginley , and J. D. Perkins, *Journal of Materials Chemistry*, **24** (2012) 3346.

[24] C. Belver, C. Adan, S. G-.Rodriguez, and M. F-.Garcia, *Chemical Engineering Journal* **224** (2013) 24.

[25] J. Im, G. Trimarchi, H. Peng, A. J. Freeman, V. Cloet, A. Raw, and K. R. Poeppelmeier, *The Journal of Chemical Physics,* **138** (2013) 194703-1.

[26] C-. M. Huang, G-. T. Pan, Y-. C. M. Li, M-. H. Li, and T. C-. K. Yang, *Applied Catalysis A: General* **358** (2009) 164.

[27] X. Hu, C. and Hu, J. Qu, *Materials Research Bulletin,* **43** (2008) 2986.

[28] X. Hu, and C. Hu, *Solid state Chemistry,* **180** (2007) 725.

[29] R. Konta, H. Kato, H. Kobayashi, and A. Kudo, *Physical Chemistry Chemical Physics*, **5** (2003) 3061.

[30] G.-T. Pan, C.-M. Huang, P.-Y. Peng, and T. C.-K. Yang, *Catalysis Today*, **164** (2011) 377.

[31] Y. C. M. Li, R. H. Tsai, and C. M. Huang, *Nanoengineering and Nanosystems*, **226** (2012) 35.

[32] C. M. Huang, L. S. Huang, Y. S. Li, I. H. Liu, and C. Y. Chang, *Sustainable Environment Research*, **21** (2011) 45.

[33] M. I. Baraton, G. Busca, M. C. Prieto, G. Ricchiardi, and V. S. Escribano, *Journal of Solid State Chemistry*, **112** (1994) 9.

[34] G. Radtke, S. Lazar, and G. A. Botton, *Physical Review B*, **74** (2006) 155117.

[35] P. D. Tsokov, V. N. Blaskov, Y. S. Stefanov, and T. M. Dobrev, *Journal of International Research Publication,* **1** (2006) 25.

[36] T. Fujii, H. Oohashi, T. Tochio, Y. Ito, A.-M. Vlaicu, and S. Fukushim, *Journal of Electron Spectroscopy and Related Phenomena*, **184** (2011) 10.

[37] S. S. Rajput, and S. Keshri, *Journal of Materials Engineering and Performance*, **23** (2014) 2103.

[38] S. H. Chuang, R. H. Gao, D. Y. Wang, H. P. Liu, L. M. Chen, and M. Y. Chiang, *The Chinese Chemical Society*, **57** (2010) 932.

[39] M. Karimipour, J. M. Wikberg, N. Shahtahmasebi, M. R. R. Abad, M. M. B.-Mohagheghi, and P. Svedlingh, *Nanoscience and nanotechnology*, **11** (2011) 1.

[40] M. K. Yadav, A. V. Kothari, and V. K. Gupta, *Dyes and Pigments*, **89** (2011) 149.

[41] G. W. Zhou, D. K. Lee, Y. H. Kim, C. W. Kim, and Y. S. Kang, *Bulletin of the Korean Chemical Society*, **27** (2006) 368.

[42] M. W. Li, X. M. gao, Y. L. Hou, and C. Y. Wang, *Nano-and Electronic physics*, **5** (2013) 03022.

[43] J. Luo, X. Xing, R. Yu, Q. Xing, D. Zhang, and X. Chen, *Journal of Alloys and compounds*, **402** (2005) 263.

[44] M. Enhessari, A. Parviz, K. Ozaee, and E. Karamali, *Experimental Nanoscience*, **5** (2010) 61.

[45] J. Wang, H. Ruan, W. Li, Y. Hu, J. Chen, Y. Shao, and Y. Zheng, *Journal of Physical Chemistry B*, **116** (2012) 13935.

[46] Y. He, L. Zhoa, Y. Wang, H. Lin, T. Li, X. Wu, and Y. Wu, *Journal of Chemical Engineering*, **169** (2011) 50.

[47] W. Y. Teoh, J. A. Scott, and R. Amal, *Journal of Physical Chemistry*, **3** (2012) 629.

[48] L. Zhanga, Y. Heb, P. Yea, W. Qina, Y. Wua, and T. Wua, *Materials Science and Engineering B*, **178** (2013) 45.

[49] B. Inceesungvorn, T. Teeranunpong, J. Nunkaew, S. Suntalelat, and D. Tantraviwat, *Catalysis Communications*, **54** (2014) 35.

[50] S. B. Rawal, S. Bera, D. Lee, D. J. Jang, and W. I. Lee, *Catalysis Science & Technology*, **3** (2013) 1822.

[51] L. Zhang, Y. He, P. Ye, Y. Wu, and T. Wu, *Journal of Alloys and Compounds*, **549** (2013) 105.

[52] S. Wang, D. Li, C. Sun, S. Yang, Y. Guan, and H. He, *Applied Catalysis B: Environmental* , **144** (2014) 885.

[53] G. Sun, H. Xu, H. Li, H. Shu, C. Liu, and Q. Zhang, *Reaction Kinetics Mechanisms and Catalysis*, **99** (2010) 471.

[54] Y. Qu, W. Zhou, and H. Fu, *ChemCatChem*, **6** (2014) 265.

[55] X. Chu, X. Liu, G. Wang, and G. Meng, *Materials Research Bulletin*, **34** (1999) 1789.

[56] B. C. Yadav, R. C. Yadav, S. Singh, P. K. Dwivedi, H. Ryu, S. Kang, *Optics and Laser Technology*, **49** (2013) 68.

[57] M. Siemons, and U. Simon, *Sensors and Actuators B*, **126** (2007) 595.

[58] T. Shukla, B. C. Yadav, and P. Tandon, *Sensor Letters*, **9** (2011) 1.